ADVANCED HEALTHCARE MATERIALS
www.advhealthmat.de

Non-Surgical, In-Stent Membrane Bioelectronics for Long-Term Intracranial Pressure Monitoring

Jimin Lee, Allison Bateman, Mi Hyeon Kim, Bruno Rigo, Hodam Kim, Jaeho Lee, Yun Hyeok Choi, Robert Herbert, Deok Hee Lee, and Woon-Hong Yeo**

Traditional intracranial pressure (ICP) monitoring methods, using intraventricular catheters, face significant limitations, including high invasiveness, discrete data, calibration complexities, and drift issues, which hinder long-term and stable monitoring. Here, a non-surgical, in-stent membrane bioelectronic system is presented for continuous and reliable ICP monitoring. This platform integrates a capacitive thin-film sensor with a stent, enabling precise real-time detection of pressure fluctuations directly within the dural venous sinus without requiring skull penetration or frequent recalibration. The sensor demonstrates a high sensitivity of 0.052%/mmHg and a broad, readable pressure range of 3–30 mmHg while maintaining calibration-free and drift-free performance. A series of in vivo studies highlight the system's superior sensitivity, rapid sampling rate, and long-term stability compared to conventional microcatheters. Statistical analyses reveal a strong agreement between the device and clinical reference, underscoring its potential to revolutionize ICP monitoring. These advancements pave the way for broader clinical applications, minimizing complications and improving patient outcomes in neurocritical care.

1. Introduction

Having real-time intracranial pressure data is vital for the clinical decision-making and management of various severe neurological conditions, including traumatic brain injury, hydrocephalus, and idiopathic intracranial hypertension. Elevated ICP can lead to severe complications, such as brain ischemia and permanent neurological damage, making real-time ICP monitoring vital for timely intervention and improved patient outcomes. Current gold-standard methods like intraparenchymal microsensors and intraventricular catheters are effective but present significant limitations due to their invasive nature, risk of infection, sensor zeroing requirement, and reliance on complex surgical procedures.[1] These conventional methods, particularly intraventricular catheters, require skull penetration, making them invasive and increasing

J. Lee, A. Bateman, H. Kim, J. Lee, W.-H. Yeo
George W. Woodruff School of Mechanical Engineering
Georgia Institute of Technology
Atlanta, GA 30332, USA
E-mail: whyeo@gatech.edu

J. Lee, A. Bateman, B. Rigo, J. Lee, W.-H. Yeo
Wearable Intelligent Systems and Healthcare Center (WISH Center) at the Institute for Matter and Systems
Georgia Institute of Technology
Atlanta, GA 30332, USA

M. H. Kim, D. H. Lee
Department of Radiology
Research Institute of Radiology
Asan Medical Center
University of Ulsan College of Medicine
88 Olympic-ro 43-gil, Songpa-gu, Seoul 05505, Republic of Korea
E-mail: dhlee@amc.seoul.kr

The ORCID identification number(s) for the author(s) of this article can be found under https://doi.org/10.1002/adhm.202404680

DOI: 10.1002/adhm.202404680

M. H. Kim
Biomedical Engineering Research Center
Asan Institute for Life Sciences
Asan Medical Center
88 Olympic-ro 43-gil, Songpa-gu, Seoul 05505, Republic of Korea

B. Rigo
School of Electrical and Computer Engineering
Georgia Institute of Technology
Atlanta, GA 30332, USA

H. Kim
Biomedical Engineering and Imaging Institute
Department of Radiology
Icahn School of Medicine at Mount Sinai
New York, NY 10029, USA

Y. H. Choi
Department of Neurosurgery
Haeundae Paik Hospital
875, Haeun-daero, Haeundae-gu, Busan 48108, Republic of Korea

R. Herbert
Department of Mechanical and Industrial Engineering
Louisiana State University
Baton Rouge, LA 70803, USA

W.-H. Yeo
Wallace H. Coulter Department of Biomedical Engineering
Georgia Institute of Technology and Emory University School of Medicine
Atlanta, GA 30332, USA

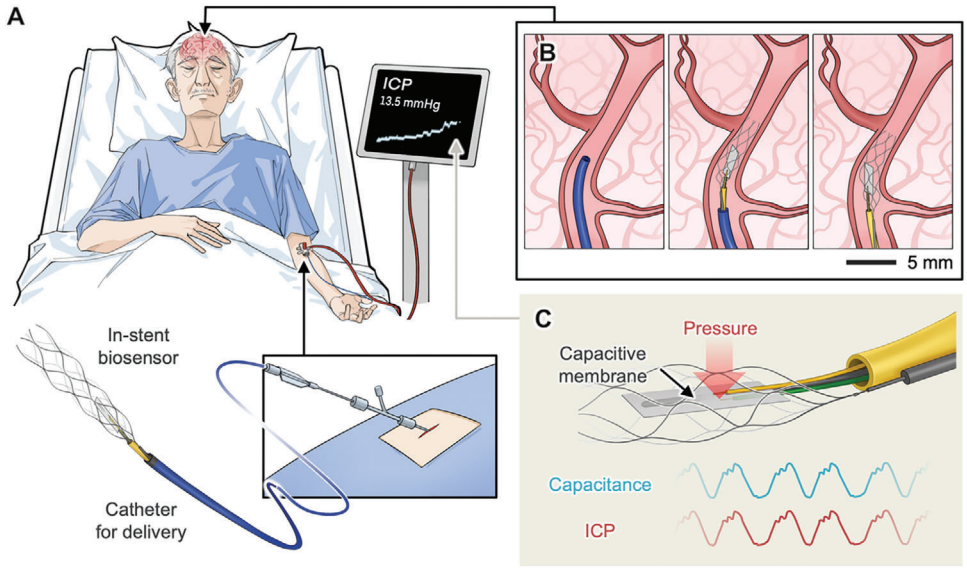

Figure 1. Overview of a non-surgical membrane bioelectronic system for continuous ICP monitoring. A) Illustration of the developed in-stent biosensor system loaded into a catheter and delivered through the venous system from the antecubital vein to the superior sagittal sinus, offering continuous, long-term ICP monitoring without skull penetration. B) Capacitive membrane sensor-integrated stent navigated through veins smaller than 4 mm and seamlessly deployed in the superior sagittal sinus. C) Principle of detecting ICP values via the measurements of capacitance changes by the membrane sensor.

the risk of complications such as infection rates up to 25% and hemorrhage risks between 5% and 7%. Furthermore, these systems are restricted to intensive care settings and are unsuitable for long-term, non-invasive monitoring, limiting their applicability in broader clinical scenarios, such as outpatient care.[2–4]

Recent advancements in wireless telemetry systems, such as near-field communication, inductive coupling, and ultrasonic telemetry, offer minimally invasive alternatives.[5] However, these systems face major challenges, including signal attenuation caused by biological tissues, cerebrospinal fluid, and the skull. Their reduced readout range and dependency on close-range external receivers further limit their clinical utility.[6] Besides, device size limitations make it difficult to integrate these systems into small anatomical spaces, such as brain arteries, without compromising performance. Amid these challenges, endovascular approaches offer a promising, minimally invasive alternative.[7] Unlike traditional methods that require cranial penetration, angiographic techniques involve minimal incisions, reduced need for general anesthesia, and faster recovery times. These catheter-based procedures enable precise device placement and real-time imaging, significantly improving treatment accuracy and patient safety, thereby better tolerated in the conscious patient. The endovascular methods also allow for the navigation of complex anatomical structures, further enhancing their appeal as a minimally invasive solution for ICP monitoring. Drawing on this framework, the development of a minimally invasive intravascular pressure sensing system could achieve the "holy grail" in neurocritical care as a significant advancement to address the limitations of current ICP monitoring methods.[4]

Here, in response to the growing need for safer, less invasive ICP monitoring solutions, we propose a thin-film sensor-integrated endovascular stent platform. This system offers a minimally invasive approach for real-time, continuous ICP monitoring. Our design incorporates an ultra-thin capacitive nanomembrane sensor mounted on a self-expanding stent retriever, which can be deployed via retrograde venous access. The sensor is engineered to detect subtle pressure changes within the dural venous sinus, providing a precise surrogate measurement of ICP. This approach circumvents the need for traditional, highly invasive cranial procedures and is compatible with existing catheter delivery systems, making it suitable for broader clinical use. The wired stent-sensor platform is designed to capture both static and dynamic pressure changes, including pulsatile variations, with high sensitivity. Integrating the sensor with a self-expanding stent ensures stable, long-term positioning within the dural venous sinus (DVS), enabling continuous monitoring without the need for complex wireless systems or frequent recalibration. The capacitive design of the sensor allows it to detect pressure changes as small as 15 mmHg, reflecting normal ICP levels (i.e., 5–15 mmHg)[3,4,8] while maintaining a rapid response time to capture pulsatile pressure variations.

2. Results and Discussion

2.1. Overview of the Non-Surgical, In-Stent Membrane Bioelectronics

Figure 1A illustrates our non-surgical system for continuous ICP monitoring, using an ultra-thin, capacitive sensor integrated with

W.-H. Yeo
Parker H. Petit Institute for Bioengineering and Biosciences
Georgia Institute of Technology
Atlanta, GA 30332, USA

a stent platform. This design provides a minimally invasive alternative to conventional ICP methods, allowing accurate, less painful measurements without the need for skull penetration. Unlike wireless sensors that suffer from signal interference due to cerebrospinal fluid, brain tissue, or skull, our wired system ensures reliable, uninterrupted monitoring. A 170 cm fully insulated conductive wire, that runs from the antecubital vein to the superior sagittal sinus (SSS), is electrically connected with a highly sensitive ultra-thin capacitive sensor at the end of the wire. This setup allows continuous ICP monitoring without the need for complex wireless implants. Signals are transmitted through the exposed end of the wire near the antecubital vein, ensuring stable and precise data acquisition over extended periods, overcoming the limitations of wireless systems that often require implanting circuits near the lesion. The sensing platform should be miniaturized enough to enable proper placement within the body, ensuring compatibility with implantation techniques and anatomical limitations.[11] As depicted in Figure 1B, the sensor-integrated stent platform, loaded into a catheter, smoothly navigates through tortuous veins smaller than 4 mm (e.g., from the antecubital vein to the brachial vein, subclavian vein, and internal jugular vein) to its final destination in the SSS. Once seamlessly deployed, the stent expands from a compressed state within the catheter to a final diameter of 4 mm, ensuring stable positioning for effective ICP monitoring. This confirms the compatibility of the device with small anatomical spaces, making it suitable for smooth deployment within the SSS (see Figure S7 (Supporting Information) for the lumen diameter diagram showing the relative sizes of the target lesion and sensor platform).[12] This system reduces the need for invasive cranial procedures, while the high-sensitivity thin-film sensor accurately detects pressure variation based on a change in its capacitance (Figure 1C). The platform also ensures long-term, continuous monitoring of static and pulsatile pressure variations, significantly improving patient safety and comfort.

2.2. Sensor Fabrication and Device Integration

Implantable sensors typically require hydrophobic surface treatments achieved through plasma treatments or chemical modifications. However, since our sensor is integrated into a stent and delivered via catheter, no additional surface treatment was required. Instead, we focused on ensuring biocompatibility through a parylene coating, which effectively mitigates the risk of polymer resin residues and contamination. As shown in **Figure** 2A, the capacitive membrane sensor is electrically connected to the tip of a 170 cm guidewire, allowing precise detection of external pressure changes and corresponding capacitance variations. The ultra-thin, flexible membrane sensor is securely attached to the endovascular stent mesh using medical-grade adhesive, ensuring stable deployment and preventing sensor-stent separation (Figure 2B; see Figure S8, Movie S1, Supporting Information). This design eliminates signal collection issues related to sensor detachment from the stent and ensures electrical insulation between the sensor-connected guidewire and the push wire of the stent, preventing interference. Figure 2C–E present the dimensions and structure of the capacitive sensor. The dielectric layer was fabricated from polydimethylsiloxane (PDMS) micropyramids, using electroforming and plating processes to create a microfabricated thin-film substrate. A capacitive sensor's sensitivity and response to pressure are highly dependent on the mechanical properties of the dielectric material between its conductive plates. A key factor is the force required to compress the dielectric. As the dielectric deforms, it brings the conductive plates closer together, increasing the value of its capacitance. Materials that deform more easily under minimal force allow the sensor to respond more rapidly to pressure changes. For optimal performance, the sensor must also exhibit elastic behavior, ensuring it can return to its original shape and baseline capacitance value after deformation. To enhance the sensitivity of the capacitive sensor, efforts such as geometric parameter optimization were implemented.[13] By tailoring the deformation characteristics of the micropyramidal microstructure under applied pressure, we aimed to maximize sensitivity. Given the high precision required for intracranial pressure monitoring, achieving exceptional sensitivity with minimal error margins was essential. This optimization resulted in significantly enhanced sensitivity, particularly in the low-pressure range, consistent with trends observed in prior studies (e.g., micropyramid > micropillar > planar).[14] Additionally, to improve the dielectric properties, porosity was incorporated within the micropyramidal PDMS dielectric layer. Combined with the inherently low Young's modulus and high dielectric constant of PDMS, these features significantly enhanced the sensor's ability to detect subtle pressure changes with high accuracy.[15] The resulting structure was highly optimized for insertion into cerebral vasculature, with minimal thickness (300 μm), width (0.4 mm), and length (6 mm) (Figure 2C). The sensor comprises two metallic layers sandwiching the PDMS dielectric layer (Figure 2D). When pressure is applied perpendicularly to blood flow, the contact area between the upper metal layer and the PDMS changes, inducing capacitance variation. The strategic placement of the membrane sensor near the edge of the stent enhances sensitivity, maximizing capacitance fluctuations in response to pressure changes. Figure 2E illustrates the morphological features of the micropyramidal PDMS dielectric layer. A template stamping process produced a uniform structure with a base of 100 μm, a height of 100 μm, and a pitch of 150 μm. Additionally, we introduced a porous structure on the micro pyramidal surface using a solution evaporation process (isopropyl alcohol:acetone = 60:40 vol%), which further improves the sensing performance (see Figures S9,S10, Supporting Information for the comparison between porous- and non-porous PDMS structures in morphology, and reproducibility of the sensor fabrication process, respectively).[16] Comparative data in capacitance between porous and non-porous PDMS structures will be discussed in detail. The fabricated stent-sensor platform can be reliably delivered through a 4.2 french size (Fr) Fubuki catheter without the need for additional surface treatments (Figure 2F). When compressed inside the catheter, the diameter of the stent is ≈<1.3 mm, expanding to 4 mm upon deployment in the dural venous sinus. Even after repeated cycles of compression and dilatation, the ultra-thin nanomembrane capacitive sensor exhibited no morphological damage. Biocompatibility is key to the longevity and performance of implantable sensors. Figure S11 (Supporting Information) shows the biocompatibility test results for the materials used in the capacitive sensor fabrication, with parylene C commonly employed for

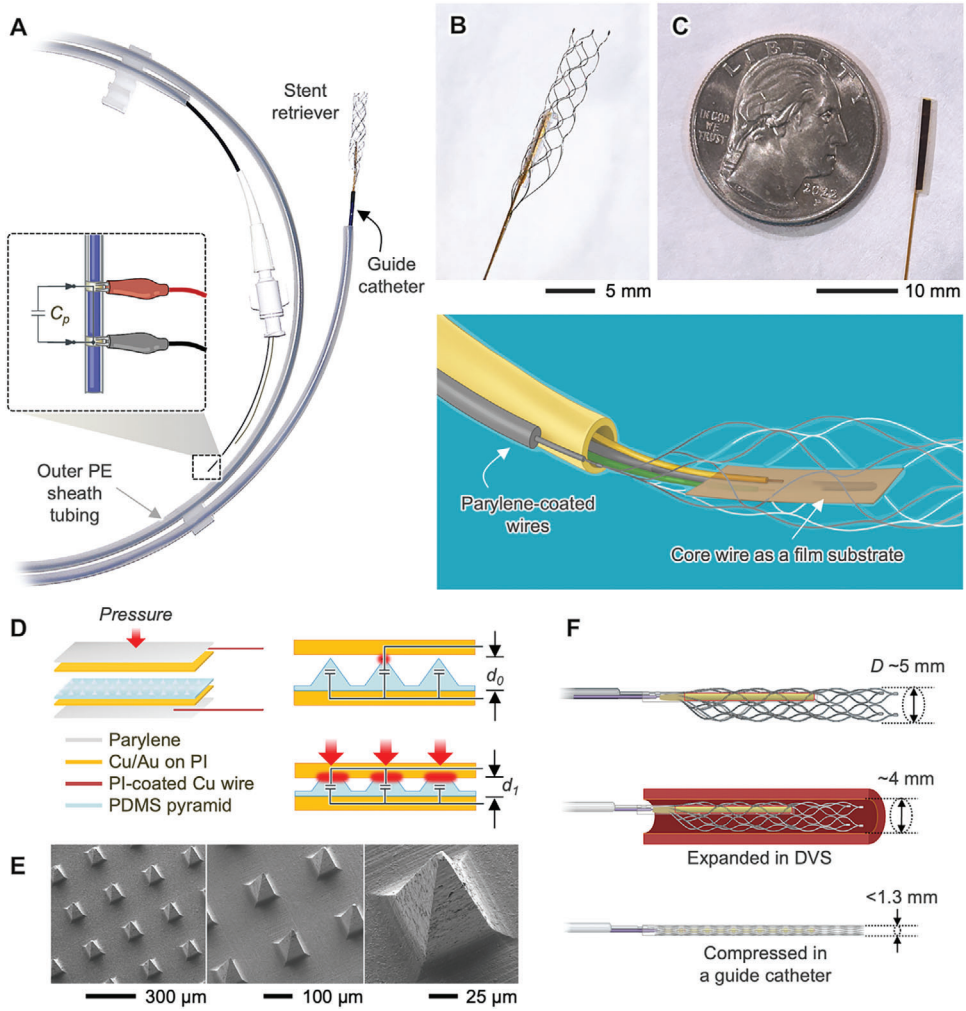

Figure 2. Membrane sensor-integrated stent system. A) Photo of the in-stent biosensor system, which is deployable within a blood vessel using a 4.2-Fr guide catheter. B, C) Photos and illustration of a fabricated in-stent biosensor system that has an exceptionally smaller form factor. D) Schematic illustration of the structural layout and working principle of the membrane pressure detecting sensor. E) SEM images of the PDMS micro pyramidal structures used as a dielectric layer in the pressure sensor. F) Changes in the diameter of the membrane sensor-integrated vascular stent during expansion (top), deployment in the blood vessel (middle), and compression (bottom).

encapsulation.[17] According to ISO standards, materials demonstrating over 70% cell viability are deemed biocompatible and non-toxic.[18] The positive control was 1% sodium dodecyl sulfate, a substance that kills cells through lysis, which is evident by its significantly low cell viability of 6.7%. The negative control consisted of untreated cells in plain medium, showing 100% cell viability, serving as a baseline for comparison. The tested samples, which were fully encapsulated by biocompatible materials such as PDMS, parylene C, and PI, showed cell viability of up to 84.90%, while the one-side Cu membrane showed only 57.51%. The polymer-covered samples met the ISO standard with cell viabilities exceeding 70%, confirming their suitability for long-term implantation, and highlighting the importance of encapsulation. The biocompatibility results suggest that the materials used in the sensor are appropriate for safe, long-term implantation in medical devices.

2.3. In Vitro Validation of the Device's Performance

Figure 3A shows the overview of the in vitro setup to validate the fabricated device's performance in detecting ICP. Details of the system setup showing a custom-built intracranial phantom appear in Figure S5 (Supporting Information). This model was designed to replicate the critical features of the intracranial cavity and the dural venous sinus (DVS), providing a controlled environment to assess the sensor accuracy, sensitivity, and response to varying pressure levels. The phantom included key intracranial components—a rigid skull, a DVS, and a brain compartment filled with 0.08 M saline solution—while maintaining a closed fluid circuit using a pulsatile flow pump to simulate venous blood flow. The sensor, integrated with a commercial stent and deployed in the DVS section (Figure 3B and see Movie S2, Supporting Information), was tested under varying pulsatile

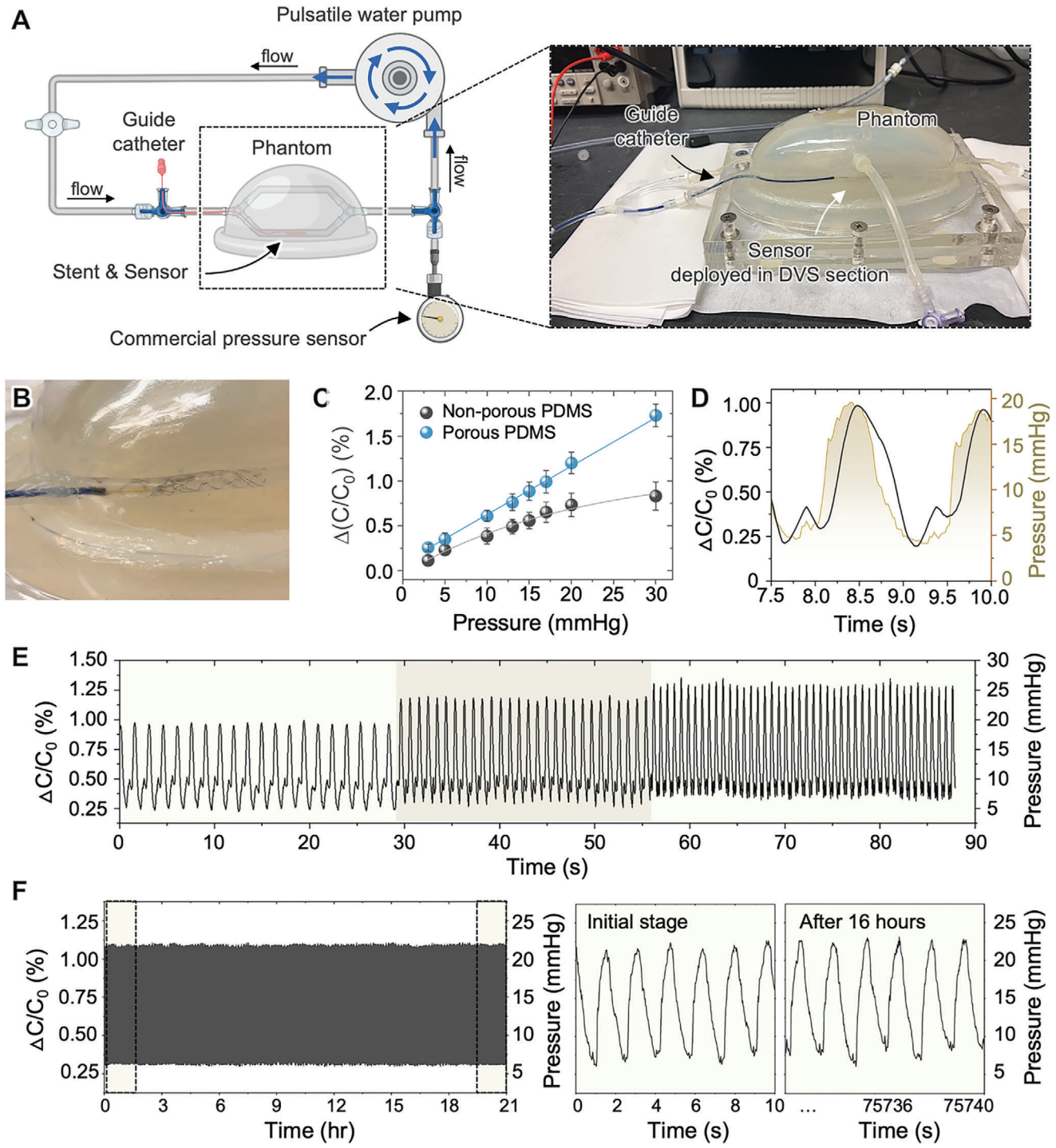

Figure 3. In vitro validation of ICP monitoring using an artery phantom. A) Scheme of the testing setup with a pulsatile water pump and an artery phantom. B) Expanded view of the 0.4-mm-wide sensor-integrated stent deployed in the dural venous sinus section of the phantom. C) Sensitivity comparison between non-porous and porous PDMS dielectric layers. D) Response and recovery time of the sensor upon pressure application. E) Repeatability test of the sensor under pulsatile conditions (40, 60, 80 bpm applied). F) Durability test of pressure detection under 50000 loading cycles with 40 bpm.

conditions to validate its functionality and long-term stability. The sensing performance of the thin-film sensor was evaluated across a pressure range from 3 to 30 mmHg. As shown in Figure 3C, we compared the sensitivity of two different thin-film sensors, which incorporate either porous- or non-porous PDMS dielectric layers. The porous micro pyramidal PDMS layer exhibited significantly higher sensitivity, with a capacitance change rate of 0.052%/mmHg, compared to 0.028%/mmHg for the non-porous PDMS layer. This enhanced sensitivity of the porous layer can be attributed to its increased surface area, which facilitates greater deformation under applied pressure, resulting in a more pronounced change in capacitance. The linear response observed in both cases confirm the sensing capability to detect ICP variations accurately within the physiological range. The response time, defined as the duration required for the sensor to detect a change in pressure, was also evaluated. As shown in Figure 3D, the sensor demonstrated an exceptionally fast response time of ≈<0.2 s, with equally rapid recovery. This fast response is crucial for capturing dynamic changes in ICP, particularly pulsatile variations, which occur on short timescales. The ability to measure rapid pressure fluctuations ensures that the sensor can provide real-time monitoring and timely feedback in critical care settings. Figure 3E,F illustrate the results of pulsatile testing under cyclic loading. The sensor was subjected to pressure cycles simulating physiological conditions, ranging from 40 to 80 beats per minute (bpm). The sensor maintained excellent repeatability across multiple cycles, with consistent changes in capacitance correlating with the applied pressure. This confirms the stability and accuracy of the sensor in monitoring pulsatile ICP variations over time. Furthermore, long-term durability testing (Figure 3F) demonstrated the sensing ability to withstand 50000 loading cycles without significant degradation in performance. After 21 h of continuous cyclic testing, the sensor still exhibited reliable and repeatable output, highlighting its robustness for long-term monitoring applications. The in vitro results validate the sensing capability to continuously and accurately monitor both static and pulsatile ICP variations. This is a significant improvement over traditional monitoring methods, which often focus solely on mean ICP values.[3] To simulate capacitance changes caused by natural bending in cerebral vasculature, bending tests were conducted using the setup in Figure 3A with silicone tubing (Figure S12A–C, Supporting Information). The in-stent thin-film sensor was bent at angles of 0°, 10°, and 20° under pulsed pressure (30 mmHg). Subtle changes in absolute capacitance and minor variations in relative capacitance ($\Delta C/C_n$) were observed, likely due to deformation of the micropyramidal PDMS layer. For accurate measurements in anatomical contexts, the bending angles of the thin-film sensor can be monitored in real-time during stent deployment using angiographic guidance, ensuring precise alignment of the membrane sensor with the endovascular stent mesh. A calibration equation, shown in Figure S12D (Supporting Information), based on bending angles can then be applied to correct capacitance readings, ensuring reliable performance in complex vascular environments. Overall, our sensor's ability to capture both static and dynamic changes offers a more comprehensive view of intracranial dynamics. The in vitro evaluation also demonstrates that the sensor offers high sensitivity, rapid response, and long-term stability, making it a promising tool for continuous ICP monitoring in both clinical and remote settings.

2.4. In Vivo Validation of the Device's Performance

Figure 4 shows the result of a set of in vivo studies that validate our device's performance with a swine model, selected for its physiological similarity to human intracranial conditions. Details of the setup appear in Figure S13 (Supporting Information). This study was crucial for validating the precision, reliability, and effectiveness of the sensor in real-time monitoring of ICP changes. The in vivo test results highlight the potential of our stent-based system, especially when navigating complex anatomical structures, while demonstrating its minimally invasive nature compared to traditional ICP monitoring systems, such as the Codman MicroSensor. As depicted in Figure 4A, B, the experimental setup involved a dual approach. A commercial transducer and silicone balloon catheter (SBC) were inserted via a burr hole in the skull to modulate ICP levels, while the sensor-integrated stent was deployed via the femoral vein using a guide catheter, with the microcatheter serving as the reference electrode (see Figures S14,S15, Supporting Information for the detailed setup and deployment). The stent system was successfully navigated to the DVS through the femoral vein, with angiographic imaging confirming accurate positioning and deployment of the stent with four distal radiopaque markers (Figure 4C–E; Figure S16, Supporting Information). The SBC was inserted into the subdural space (Figure 4B), and its inflation was used to manipulate ICP levels, ranging from normal levels (5–15 mmHg) to elevated states, which is up to 30 mmHg. Notably, ICP can be measured indirectly through the DVS pressure. Rooted in the Monro-Kellie doctrine, which asserts that intracranial pressure remains constant within the fixed volume of the cranial cavity, recent studies have shown a strong correlation between lumbar opening pressure and sinus pressure.[19] This suggests that pressure measurements taken from the DVS could serve as a viable surrogate for direct ICP measurements, enabling minimally invasive monitoring without penetrating the brain parenchyma. **Figure 5A** shows the setup for continuous ICP readings, which were recorded in parallel using both the microcatheter reference sensor and the thin-film sensor integrated into the stent (Figure S17, Table S1, Supporting Information for a comparison of measurement methods). Since the data from the Codman and microcatheter systems was not automatically collected or saved, we recorded both screens and manually extracted the data at 0.2-s intervals for Codman and 1-s intervals for the microcatheter. The data were collected focused on ICP levels of 0 to 20 mmHg by inflating the balloon. The ICP measurements from both the reference microcatheter (red trace) and the thin-film sensor (blue trace) are presented in Figure 5B. The data reveal that the thin-film sensor closely tracked the reference measurements, with both sensors displaying a clear response to gradual increases in ICP during balloon inflation. The thin-film sensor exhibited high sensitivity, consistently aligning with the reference values. Figure 5C provides a more detailed view of the sensor performance during the in vivo study, highlighting several advantages of the thin-film sensor over the reference system. The thin-film sensor demonstrated greater continuity in the data, enabled by its higher sampling rate, which allows for more precise tracking of rapid pressure changes. This, combined with the narrower error range, highlights the enhanced sensitivity of the sensor, particularly in detecting subtle pressure variations. These

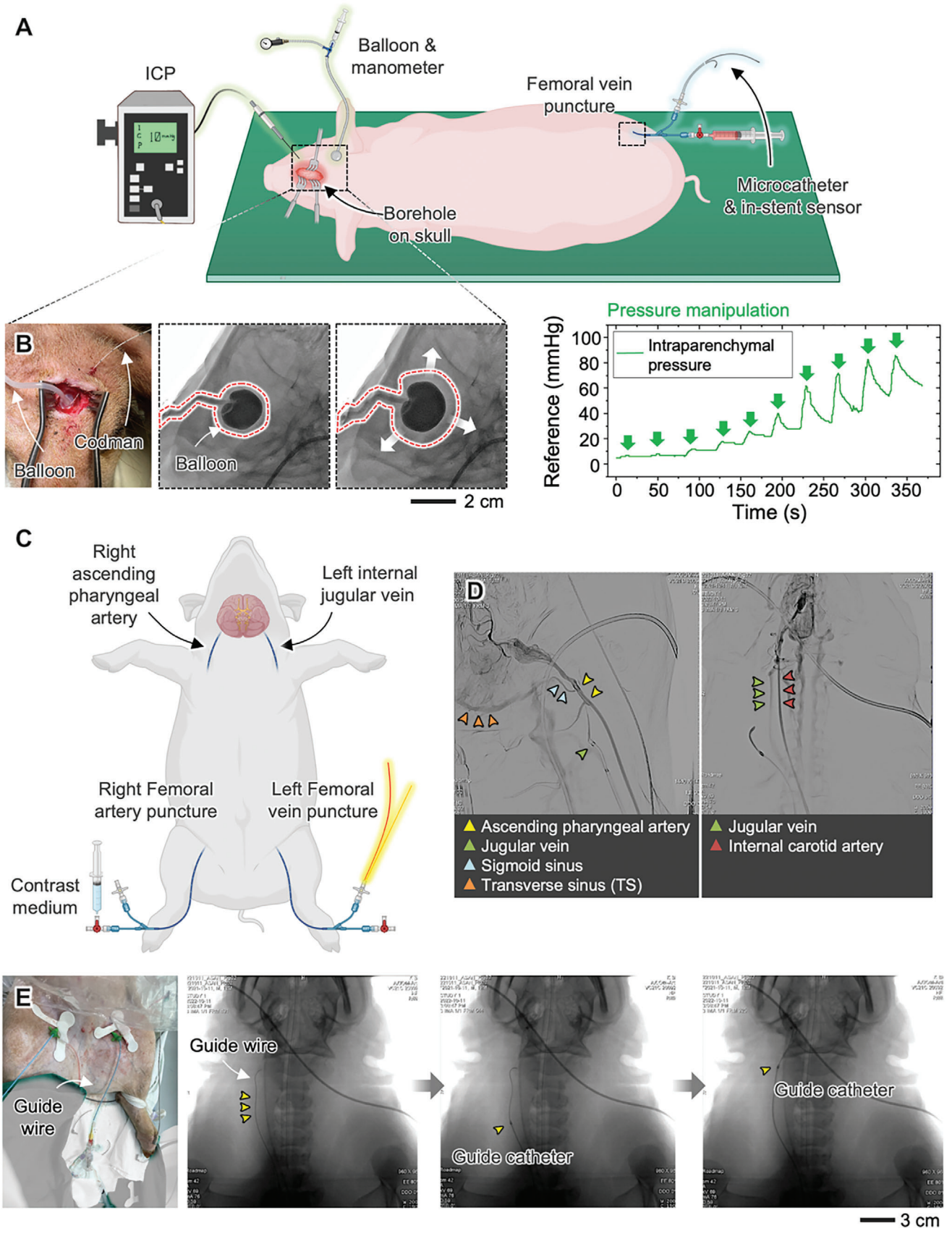

improvements make the thin-film sensor more accurate and capable of delivering higher-resolution data, which is crucial for real-time monitoring of both dynamic and mean ICP fluctuations. Notably, the performance of the thin-film sensor aligns with the standards set by the American National Standards Institute and the Association for the Advancement of Medical Instrumentation, which recommend a reading difference of only 2 mmHg for ICP values between 0 and 20 mmHg, and less than 10% for ICP values between 20 and 100 mmHg.[4] This high level of accuracy underscores the novelty of our sensor and its potential to surpass current monitoring technologies. Given the successful performance of these devices in the intracranial space, their application could extend to other organs and compartments of the body. As demonstrated in the in vitro studies, the soft, thin-film sensor is capable of detecting pulsatile ICP, which could significantly enhance our understanding of secondary brain injury.[20] To quantify the accuracy of the thin-film sensor compared to the reference microcatheter, we determined a statistical significance by performing Spearman correlation analysis and Bland-Altman analysis. As shown in Figure 5D, the Spearman correlation coefficient shows a tight linear correlation ($r = 0.90578$, $p < 0.001$), indicating a high level of positive agreement between the two systems (see Table S2, Supporting Information for Spearman's rank correlation coefficients). The Bland–Altman plot in Figure 5E further supports this, with most data points falling within the 95% confidence interval (CI). The mean bias between the thin-film sensor and the reference was −0.1738 (95% CI: −1.1268 to 0.7791), indicating that the differences between the two-sensor ICP monitoring were within acceptable limits, reinforcing the reliability of the thin-film sensor. Notably, the intraclass correlation coefficient was 0.7958, indicating strong agreement between the two methods (see Table S3, Supporting Information for detailed Bland-Altman analysis results for each phase). The seamless integration of the thin-film sensor into the stent enabled stable deployment and continuous, real-time monitoring throughout the experiment. The system demonstrated high reliability and repeatability in data collection, with no technical complications arising from wire handling or sensor stability. This performance stands in stark contrast to the 021 microcatheter, which encountered significant challenges. Specifically, technical difficulties in stable microcatheter tip positioning in the transverse sinus prevented it from accurately measuring ICP in this critical region (Figure S18, Supporting Information). These issues highlight the limitations of conventional systems when navigating anatomically constrained areas, further underscoring the superior adaptability of the thin-film sensor. The miniaturized dimensions and flexibility of the thin-film sensor allowed it to overcome the challenges posed by anatomical variations, successfully capturing continuous ICP data even in locations that are difficult to access. This capability, combined with a high sampling rate (e.g., up to 20/s) and real-time data transmission, positions the stent-based sensor as a transformative tool for ICP monitoring in both standard and complex clinical scenarios. Table S1 (Supporting Information) compares the ICP measurement methods used in this study, including the proposed stent-sensor platform, microcatheter, and Codman system. The thin-film sensor consistently outperformed its counterparts across key metrics, including sampling rate, sensitivity, invasiveness, and the ability to record, save, and transfer data for further analysis. This comprehensive comparison illustrates the distinct advantages of the proposed system, which offers a robust, minimally invasive solution for continuous ICP monitoring. Following the in vivo experiment, the sensor was retrieved and re-evaluated for performance across a pressure range of 3 to 30 mmHg. As shown in Figure S19 (Supporting Information), the sensor maintained a nearly identical slope in capacitance changes, indicating consistent sensitivity before and after the study. The slight sensitivity variation ($\Delta = 0.0497\%$/mmHg after the study vs $\Delta = 0.052\%$/mmHg before) suggests minimal impact from in vivo conditions. After 30 days post-retrieval, the sensor showed a negligible drift, with a sensitivity of $\Delta = 0.0472\%$/mmHg, reflecting <0.1% drift. Further analysis involved disassembling the sensor to investigate the microstructural changes in the dielectric PDMS layer. Microstructural imaging (Figure S20, Supporting Information) revealed the development of pastry-like patterns. This pattern was observed in both sensors retrieved after the in vivo study and those tested under in vitro long-term cyclic tests, implying that it can be attributed to the pressure exerted by fluid flow within the tubing during the experiment. Interestingly, despite some wear at the apexes of the micropyramids, the sensitivity of the sensor did not decline. This resilience can likely be attributed to the formation of micropores in the dielectric layer, which may have compensated for the material degradation, preserving the overall performance.

In clinical settings, wired ICP monitoring is generally utilized for short-term applications (3–6 h). Considering the procedural duration of ≈3 h per session (including stent deployment and retrieval), our sensitivity and drift data sufficiently support the system's reliability for its intended use. Even after 30 days post-retrieval, the sensor exhibited a sensitivity of $\Delta = 0.0472\%$/mmHg with a negligible drift of <0.1%. Further microstructural analysis of the dielectric PDMS layer revealed pastry-like patterns formed due to fluid pressure, as shown in Figure S20 (Supporting Information). Notably, despite minor wear at the micro pyramid apexes, the sensor maintained high sensitivity, attributed to compensatory micropore formation in the dielectric layer. These results underscore the robustness and reliability of the thin-film sensor for short-term clinical monitoring and its potential for longer durations under controlled

Figure 4. Preclinical study of the system with a swine model. A) Experimental setup showing a commercial transducer and silicone balloon catheter (for manually controlling ICP levels) via a borehole in the skull, alongside microcatheter and sensor-integrated stent deployment via the femoral vein, using a guide catheter. B) Balloon placed in the subdural area before and after dilatation. C) Schematic representation of the vascular access points and catheter placements in a sacrificial animal model. For anatomical verification of the venous structure, a catheter is positioned in the right ascending pharyngeal artery via right femoral artery puncture, followed by contrast medium injection. The left femoral vein is punctured for the insertion of the in-stent sensor and microcatheter, which are navigated through the jugular vein and positioned in the transverse sinus. D) Angiographic views of the porcine ascending pharyngeal artery, jugular vein, and internal carotid artery. E) Actual surgical setup with a 6 Fr guide wire and catheter (left) and angiographic images confirming successful stent deployment, with four distal radiopaque markers visible (right).

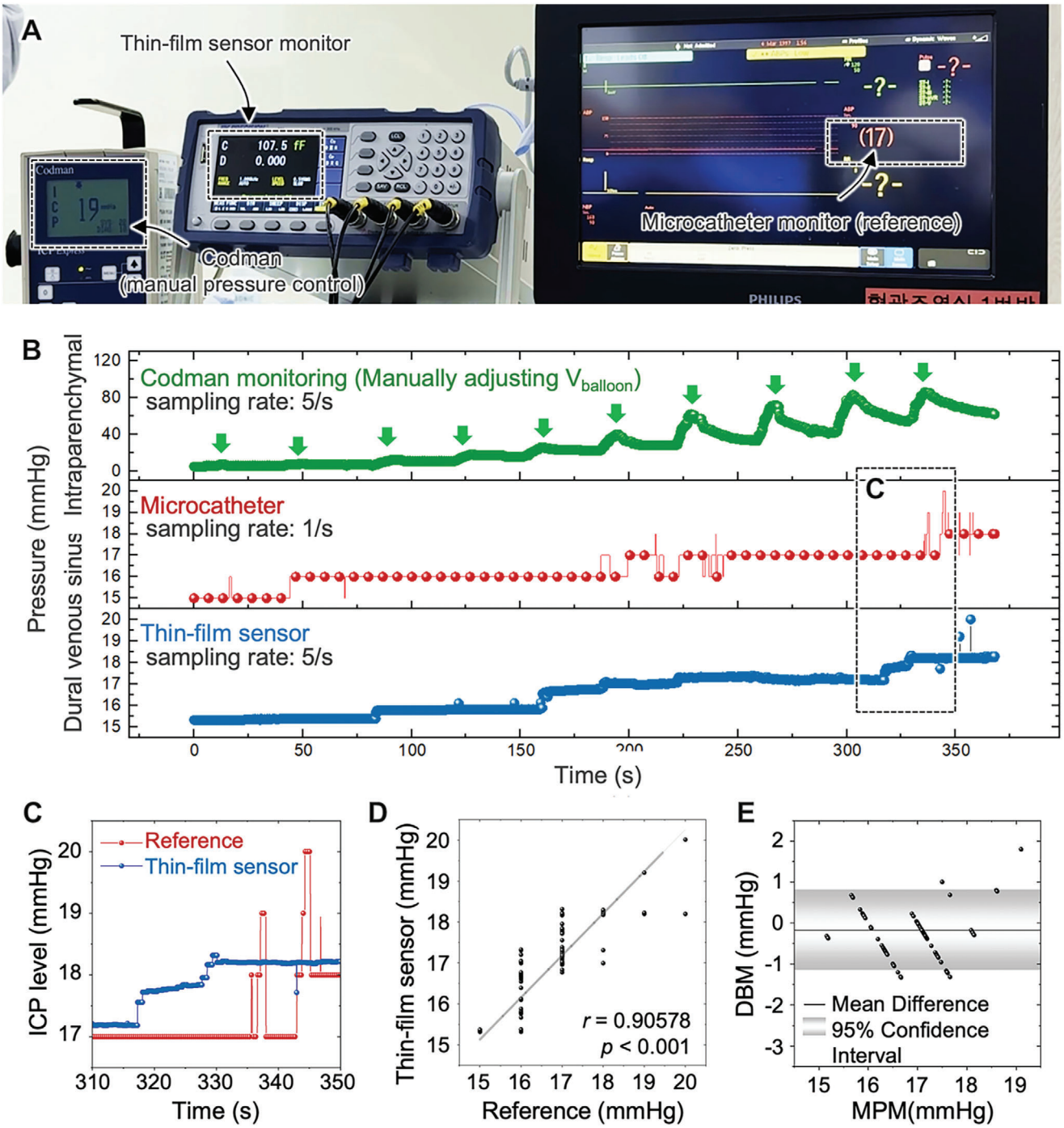

Figure 5. In vivo validation of the device's performance. A) Three representative monitors connected to the Codman transducer (left), the thin-film sensor (middle), and the microcatheter (right). B) Trace of mean ICP values obtained from the commercial monitor (green), the reference microcatheter (red), and the thin-film sensor (blue). C) Expanded view of the ICP monitoring comparing two sensors. D) Correlation between reference sensor and thin-film sensor, showing Spearman correlation coefficient, r. E) Bland-Altman plot comparing reference sensor and thin-film sensor (DBM: the difference between a pair of measurements and MPM: mean for a pair of measurements).

conditions. **Table 1** provides a comparison of our work with other studies focused on developing pressure sensors for various biomedical applications. Our sensor features a more compact design that does not require open surgery for deployment, and it provides higher sensitivity with minimal drift, allowing for the detection of small ICP changes during long-term monitoring. It shows a strong correlation with the conventional microcatheter, achieving a Spearman correlation coefficient of r = 0.906. With

Table 1. Comparison of various sensor systems for in vivo pressure monitoring.

Reference	Target pressure (typical lumen diameter)	Sensor width [mm]	Open surgery required	Long-term stability [day]	Correlation accuracy[a)]	Sensitivity, $\Delta(C/C_0)\%$/mmHg	Error range[b)] [%]
This work	Intracranial pressure [2–4 mm]	0.4	No	30	0.906	0.052	0.2
[21]		2.8	Yes	2	–	0.028	1.7
[22]		1.4	Yes	–	–	–	–
[23]		2.0	Yes	–	–	–	–
[24]		2.5	Yes	22	–	–	<15
[25]		8	Yes	2	–	–	–
[26]		9	Yes	–	–	–	–
[27]		34	Yes	0.08	0.829	–	–
[28]	Intravascular pressure [5–30 mm]	15	Yes	–	–	0.004[c)]	2.8
[29]		40	Yes	2.5	–	0.045	0.3

[a)] Highest Spearman correlation coefficient with $p < 0.001$; [b)] A reading difference of only 2 mmHg (10%) for ICP values between 0 and 20 mmHg is recommended.[4]
[c)] Sensitivity or drift values were deduced from the capacitance response to pressure.

successful in vivo testing, it shows strong potential as a promising candidate for continuous pressure monitoring in clinical settings.

3. Conclusion

This paper introduces a membrane-sensor integrated endovascular bioelectronic system, demonstrating continuous, real-time ICP readings across a range of 3–30 mmHg. The successful deployment of the device in a live pig model captures its compatibility with standard catheter delivery systems, showing comparable performance to traditional hardwired sensors. This result suggests that our sensor platform could feasibly replace conventional methods in short-term and long-term ICP monitoring, particularly for patients requiring continuous pressure measurements over several days to a month. Moreover, the low-profile design of the sensor makes it highly adaptable to clinical environments, minimizing the need for complex surgical interventions. As neurocritical care increasingly focuses on less invasive solutions, our in-stent sensor system represents a significant advancement. Its ability to monitor compartment pressure gradients continuously, without the risks associated with invasive ICP monitoring, makes it a valuable tool for managing conditions like traumatic brain injury, idiopathic intracranial hypertension, and hydrocephalus. Moreover, its ability to capture both static and pulsatile ICP provides a more complete assessment of intracranial dynamics, offering critical insights that current methods overlook. Collectively, we envision that this bioelectronic system presents a promising, cost-effective alternative to conventional ICP monitoring, with broad applications in managing neurological conditions and improving patient outcomes.

4. Experimental Section

Fabrication of Membrane Sensors: The fabrication process for the thin-film sensor involves three primary steps (Figure S1, Supporting Information): top-layer fabrication, micropyramidal dielectric layer-included bottom-layer fabrication, and final assembly. The process began with a glass substrate that serves as the base for spin-coating and curing a polyimide (PI) layer. After curing, a thin layer of gold (Au) was sputtered onto the polyimide surface. The entire layer was peeled off the glass substrate, resulting in a flexible, conductive top layer. The bottom layer was fabricated using a patterned mold to create a microstructural surface. Polydimethylsiloxane (PDMS, Sylgard 184, Dow Corning) was spin-coated and cured on the patterned mold, followed by electroforming copper (Cu) onto the flat PDMS surface. Au was then electrodeposited onto the Cu to provide the conductive base and biocompatibility (Figure S2, Supporting Information). After the mold was removed, the top and bottom layers were assembled by aligning the microstructures and bonding the two layers together. The assembled layers form the capacitive structure, where changes in pressure induce variations in capacitance. The sensor was electrically connected to a guidewire containing insulated wires (see Figures S3,S4, Supporting Information for the dimensions of the guide wire). PDMS was coated over all electrical connections and cured at 180 °C to ensure encapsulation. Finally, the entire thin-film sensor was insulated with a 5 µm biocompatible layer of Parylene C (Laboter 3; Specialty Coating Systems) to enhance durability and biocompatibility. To validate the repeatability of the microstructure, five sets of non-porous and porous micropyramidal PDMS membranes were fabricated and characterized for surface morphology and capacitive performance under varying applied pressures.

Characterization of Membrane Sensors: To investigate the microstructural characteristics of the fabricated thin-film sensor, a scanning electron microscope (FE-SEM, SU8230, Hitachi) equipped with Energy-Dispersive X-ray Spectroscopy (EDS) was employed. The surface morphology was also examined using a digital microscope (VHX-7000, Keyence). In vitro cytotoxicity evaluation of the thin-film sensor using L929 mouse fibroblasts was performed to verify biocompatibility. The adhered L929 mouse fibroblasts were treated with extraction from samples immersed in EMEM-based complete media for 24 h. After 24 h of immersion, the biocompatibility was assessed using an MTS tetrazolium/formazan reduction reagent. The dehydrogenase activities of the cells were quantified using an MTS assay (CellTiter 96 AQueous One Solution Cell Proliferation Assay, Promega) and BioTeK Synergy plate reader with optical density (OD) at a wavelength of $\lambda = 490$ nm. Fresh medium without sample incubation was used as a positive control. Results are presented as the average values ± S.D. ($n = 5$).

In Vitro Study: A simplified in-house cranial cavity model was developed to measure pressure within the DVS as a proxy for ICP measurement (Figure S5, Supporting Information).[9] The in vitro phantom consisted of silicone tubing connected to a pulsatile flow pump (Series 1400 Pulsatile Blood Pumps, Harvard Apparatus). To simulate cerebrovascular conditions, 0.08 M saline solution (3–4 cPs of viscosity at 21 °C, Sigma–Aldrich), which matched the conductivity of blood, was circulated through the tubing.[10] The thin-film sensor was integrated into an existing stent (Solitaire Platinum vascularization, Solitaire TM 2, revascularization device, SFR2-4-20, LOT A366610) and then loaded into a guide catheter (ASAHI FUBUKI 043, 4.2 Fr, ID 0.043″, ASAHI INTECC CO., LTD) (see

Figure S6, Supporting Information for a profile of endovascular stent). The full-fledged device was deployed into the silicone artery. For wired testing, a rotating hemostasis valve (RHV) was combined with the silicone artery to thread the wires from the implanted sensor outside the artery. For data recording, wired testing utilized an LCR meter connected to a LabVIEW program to monitor sensor capacitance. A commercial pressure sensor was placed near the stent and sensor for comparison, with a multimeter used to record voltage signals from the commercial sensor. For calibration of the pressure response, a comparison of the capacitance value of the thin-film sensor via data acquisition with pressures from the commercial sensor yielded calibration curves. Flow parameters were adjusted to simulate various conditions. The pulsatile pump operated at a varying stroke rate of 20–200, with stroke volumes at 4 mL, allowing for the testing of pressures between 30 and 1 mmHg.

In Vivo Study: After completing the in vitro study, in vivo feasibility study had been advanced in using a swine model chosen for its physiological resemblance to human intracranial conditions. Further details on the procedure can be found in the Methods (Supporting Information). All animal experiments adhered to the guidelines set by the Institutional Animal Care and Use Committee (IACUC). The ethical approval for the animal experiments was granted by IACUC at HLB bioStep Co., Ltd. (the assigned approval number for the conducted experiments is BIOSTEP IACUC 23-KE-0568).

Supporting Information

Supporting Information is available from the Wiley Online Library or from the author.

Acknowledgements

The authors acknowledged the support of the National Science Foundation (CCSS-2152638) and the WISH Center grant from the Georgia Tech Institute for Matter and Systems. The electronic devices in this work were fabricated at the Georgia Tech Institute for Matter and Systems, a member of the National Nanotechnology Coordinated Infrastructure (NNCI), which is supported by the National Science Foundation (ECCS-2025462).

Conflict of Interest

Georgia Tech has a pending US patent application regarding the materials in this paper.

Author Contributions

J.L., A.B., and M.H.K. contributed equally to this work. J.L. did conceptualization, formal analysis, methodology, wrote the original draft preparation. A.B. did conceptualization, formal analysis, methodology, wrote the original draft preparation. M.H.K. performed formal analysis, validation, wrote the original draft preparation. B.R. did formal analysis. H.K. did software, formal analysis. J.L. did formal analysis. Y.H.C. did validation, investigation. R.H. did conceptualization, methodology. D.H.L. did reviewing and editing, resources, supervision, project administration. W.-H.Y. did conceptualization, reviewing and editing, supervision, project administration, funding acquisition

Data Availability Statement

The data that support the findings of this study are available from the corresponding author upon reasonable request.

Keywords

capacitive sensors, endovascular stent, intracranial pressure, minimally invasive, porous pyramidal structure

Received: November 22, 2024
Revised: January 28, 2025
Published online: February 16, 2025

[1] S. Qvarlander, N. Sundström, J. Malm, A. Eklund, *J. Appl. Physiol.* **2013**, *115*, 1474.
[2] a) F. M. de Moraes, E. Rocha, F. C. D. Barros, F. G. R. Freitas, M. Miranda, R. A. Valiente, J. B. C. de Andrade, F. E. A. C. Neto, G. S. Silva, *Neurocritical Care* **2022**, *37*, 219; b) P. R., Maloney, G. W. Mallory, J. L. Atkinson, E. F. Wijdicks, A. A. Rabinstein, J. J. Van Gompel, *Neurocrit. Care* **2016**, *25*, 86; c) J. S. VanEpps, J. G. Younger, *Shock* **2016**, *46*, 597.
[3] K. B. Evensen, P. K. Eide, *Fluids Barriers CNS* **2020**, *17*, 34.
[4] S. Munakomi, J. M. Das, Intracranial Pressure Monitoring, [Updated 2024 Jan 23]. In: StatPearls [Internet]. Treasure Island (FL): StatPearls Publishing, Jan **2025**, https://www.ncbi.nlm.nih.gov/books/NBK542298/.
[5] a) X. Chen, B. Assadsangabi, Y. Hsiang, K. E. A. Takahata, *Adv. Sci.* **2018**, *5*, 1700560; b) Y. S. Choi, H. Jeong, R. T. Yin, R. Avila, A. Pfenniger, J. Yoo, J. Y. Lee, A. Tzavelis, Y. J. Lee, S. W. Chen, H. S. Knight, S. Kim, H. Ahn, G. Wickerson, A. Vázquez-Guardado, E. Higbee-Dempsey, B. A. Russo, M. A. Napolitano, T. J. Holleran, L. A. Razzak, A. N. Miniovich, G. Lee, B. Geist, B. Kim, S. Han, J. A. Brennan, K. Aras, S. S. Kwak, J. Kim, E. A. Waters, et al., *Science* **2022**, *376*, 1006; c) R. Herbert, M. Elsisy, B. Rigo, H. Lim, H. Kim, C. Choi, S. Kim, S. Ye, W. R. Wagner, Y. Chun, W. Yeo, *Nano Today* **2022**, *46*, 101557; d) R. Herbert, H. Lim, B. Rigo, W. Yeo, *Sci. Adv.* **2022**, *8*, eabm1175; e) P. Jin, J. Fu, F. Wang, Y. Zhang, P. Wang, X. Liu, Y. Jiao, H. Li, Y. Chen, Y. Ma, X. Feng, *Sci. Adv.* **2021**, *7*, eabg2507; f) J. Lee, S. J. Ihle, G. S. Pellegrino, H. Kim, J. Yea, C. Jeon, H. Son, C. Jin, D. Eberli, F. Schmid, B. L. Zambrano, A. F. Renz, C. Forró, H. Choi, K. Jang, R. Küng, J. Vörös, *Nat. Electron.* **2021**, *4*, 291; g) G. Matthew, S. Ira, R. Bruno, Z. Nathan, K. Sara, K. Hyeonseok, Y. Woon-Hong, *Soft Sci.* **2023**, *3*, 23; h) D. K. Piech, B. C. Johnson, K. Shen, M. M. Ghanbari, K. Y. Li, R. M. Neely, J. E. Kay, J. M. Carmena, M. M. Maharbiz, R. A. Muller, *Nat. Biomed. Eng.* **2020**, *4*, 207; i) B. Rigo, A. Bateman, J. Lee, H. Kim, Y. Lee, L. Romero, Y. C. Jang, R. Herbert, W. Yeo, *Biosensors Bioelectron.* **2023**, *241*, 115650; j) C. Shi, V. Andino-Pavlovsky, S. A. Lee, T. Costa, J. Elloian, E. E. Konofagou, K. L. Shepard, *Sci. Adv.* **2021**, *7*, eabf6312; k) S. M., Yang, J. H. Shim, H. U. Cho, T. M. Jang, G. J. Ko, J. Shim, T. H. Kim, J. Zhu, S. Park, Y. S. Kim, *Adv. Mater.* **2022**, *34*, 2108203.
[6] a) C. Howe, S. Mishra, Y.-S. Kim, Y. Chen, S.-H. Ye, W. R. Wagner, J.-W. Jeong, H.-S. Byun, J.-H. Kim, Y. Chun, W. Yeo, *ACS Nano* **2018**, *12*, 8706; b) J. S., Kroin, R. J. McCarthy, L. Stylos, K. Miesel, A. D. Ivankovich, R. D. Penn, *J. Neurosurg.* **2000**, *93*, 852.
[7] a) M. R. Lepore, M. Yoselevitz, W. C. Sternbergh, 3rd, Money SR. Minimally invasive vascular techniques. Ochsner J, **2000**, *2*, 145, PMID: 21765683; PMCID: PMC3117520; b) J. Park, B. Seo, Y. Jeong, I. A. Park, *Adv. Sci.* **2024**, *11*, 2307427.
[8] C. He, C. Teng, Z. Xiong, X. Lin, H. Li, X. Li, *Chin. Neurosurg. J.* **2023**, *9*, 212.
[9] K. Lee, M. Kim, J.-T. Yoon, Y. Song, B. Kwon, S. Hwang, J. Choi, D. Lee, *Interv. Neuroradiol.* **2022**, *30*, 57.
[10] A. R. Mohammadi, K. Chen, M. S. Mohamed Ali, K. Takahata, *Biosens. Bioelectron.* **2011**, *30*, 300.
[11] L. Yu, B. J. Kim, E. Meng, *Sensors* **2014**, *14*, 20620.
[12] a) S. C. Joseph, E. Rizk, R. S. Tubbs, in *Anatomy, Imaging and Surgery of the Intracranial Dural Venous Sinuses* (Ed.: R. S. Tubbs), Elsevier, Amsterdam, Netherlands **2020**, Ch. 25; b) D. R. Walsh, J. J. Lynch, D. T. O'Connor, D. T. Newport, J. J. E. Mulvihill, *Sci. Rep.* **2020**, *10*, 21763.
[13] a) B. Lee, J. Kim, H. Kim, C. Kim, S. Lee, *Sensors and Actuators A: Physical* **2016**, *240*, 103; b) S. R. A. Ruth, V. R. Feig, H. Tran, Z. Bao,

Adv. Funct. Mater. **2020**, *30*, 2003491; c) J. I. Yoon, K. S. Choi, S. P. Chang, *Microelectron. Eng.* **2017**, *179*, 60; d) Z. Zhang, X. Gui, Q. Hu, L. Yang, R. Yang, B. Huang, B. Yang, Z. Tang, *Adv. Electron. Mater.* **2021**, *7*, 2100174.

[14] J. Park, J. Kim, J. Hong, H. Lee, Y. Lee, S. Cho, S.-W. Kim, J. J. Kim, S. Y. Kim, H. Ko, *NPG Asia Mater.* **2018**, *10*, 163.

[15] R. Javidi, M. Moghimi Zand, S. Alizadeh Majd, *Micro Nano Syst. Lett.* **2023**, *11*, 13.

[16] a) J. Chen, H. Guo, X. He, G. Liu, Y. Xi, H. Shi, C. Hu, *ACS Appl. Mater. Interfaces* **2016**, *8*, 736; b) D. Kim, S. J. Park, S. B. Jeon, M. L. Seol, Y. K. Choi, *Adv. Electron. Mater.* **2016**, *2*, 1500331; c) K. Y. Lee, J. Chun, J. Lee, K. N. Kim, N. Kang, J. Kim, M. H. Kim, K. Shin, M. K. Gupta, J. M. Baik, *Adv. Mater.* **2014**, *26*, 5037; d) D. Zhu, S. Handschuh-Wang, X. Zhou, *J.Mater. Chem. A* **2017**, *5*, 16467.

[17] A. Bhatia, J. Hanna, T. Stuart, K. A. Kasper, D. M. Clausen, P. Gutruf, *Chem. Rev.* **2024**, *124*, 2205.

[18] I. Standard, in *Biological Evaluation of Medical Devices—Part 5: Tests for In Vitro Cytotoxicity*, International Organization for Standardization, Geneve, Switzerland **2009**.

[19] a) K. Lee, C. Kittel, J. B. Aldridge, S. Q. Wolfe, P. Brown, K. M. Fargen, *J. NeuroIntervent. Surg.* **2021**, *13*, 1162; b) S. Mascarenhas, G. H. F. Vilela, C. Carlotti, L. E. G. Damiano, W. Seluque, B. Colli, K. Tanaka, C. C. Wang, K. O. Nonaka, in *Intracranial Pressure and Brain Monitoring XIV* (Eds: M. U. Schuhmann, M. Czosnyka), Springer, Vienna, Austria **2012**, 117–120; c) T. J. Oxley, P. E. Yoo, G. S. Rind, S. M. Ronayne, C. M. S. Lee, C. Bird, V. Hampshire, R. P. Sharma, A. Morokoff, D. L. Williams, C. MacIsaac, M. E. Howard, L. Irving, I. Vrljic, C. Williams, S. E. John, F. Weissenborn, M. Dazenko, A. H. Balabanski, D. Friedenberg, A. N. Burkitt, Y. T. Wong, K. J. Drummond, P. Desmond, D. Weber, T. Denison, L. R. Hochberg, S. Mathers, T. J. Brien, C. N. May, *J.NeuroInterv. Surg.* **2021**, *13*, 102

[20] a) S. Kang, R. K. J. Murphy, S. Hwang, S. M. Lee, D. V. Harburg, N. A. Krueger, J. Shin, P. Gamble, H. Cheng, S. Yu, Z. Liu, J. G. McCall, M. Stephen, H. Ying, J. Kim, G. Park, R. C. Webb, C. H. Lee, S. Chung, D. S. Wie, A. D. Gujar, B. Vemulapalli, A. H. Kim, K. Lee, J. Cheng, Y. Huang, S. H. Lee, P. V. Braun, W. Z. Ray, J. A. Rogers, *Nature* **2016**, *530*, 71; b) M. F. Stiefel, A. Spiotta, V. H. Gracias, A. M. Garuffe, O. Guillamondegui, E. Maloney-Wilensky, S. Bloom, M. S. Grady, P. D. LeRoux, *J.neurosurg.* **2005**, *103*, 805; c) I. Timofeev, J. Nortje, P. G. Al-Rawi, P. J. Hutchinson, A. K. Gupta, *J.Cereb. Blood Flow Metab.* **2013**, *33*, 422.

[21] J.-H. Roh, K.-S. Shin, T.-H. Song, J. Kim, D.-S. Lee, *Micromachines* **2023**, *14*, 975.

[22] M. H. Behfar, E. Abada, L. Sydänheimo, K. Goldman, A. J. Fleischman, N. Gupta, L. Ukkonen, S. Roy, presented at *2016 38th Annual International Conference of the IEEE Engineering in Medicine and Biology Society (EMBC)*, Orlando, FL, USA, August **2016**, 1950.

[23] M. W. A. Khan, M. H. Behfar, T. Björninen, L. Sydänheimo, L. Ukkonen, presented at *2015 International Conference on Electromagnetics in Advanced Applications (ICEAA)*, Turin, Italy, September **2015**, 383.

[24] M. Ghannad-Rezaie, L. J. S. Yang, H. J. L. Garton, N. Chronis, *J. Microelectromech. Syst.* **2012**, *21*, 23.

[25] R. S. Karmakar, J.-C. Wang, Y.-T. Huang, K.-J. Lin, K.-C. Wei, Y.-H. Hsu, Y.-C. Huang, Y.-J. Lu, *ACS Omega* **2020**, *5*, 29342.

[26] Q. Wei, C. He, J. Chen, D. Chen, J. Wang, *IEEE Trans. Electron Devices* **2018**, *65*, 2592.

[27] S. Junior, E. B., E. E. Hamasaki, H. Y. Smaili, A. Wozniak, E. S. Y. Tristão, M. d. P. Loureiro, J. B. Milano, M. S. de Meneses, R. M. de Oliveira, R. Ramina, *Neurosurgery* **2023**, *92*, 647.

[28] G. Bécan, H. Philippe, J. Phung, B. Boutaud, M. Woytasik, D. Bouville, E. Lefeuvre, *J. Micromech. Microeng.* **2021**, *31*, 095008.

[29] P. Bingger, M. Zens, P. Woias, *Biomed. Microdevices* **2012**, *14*, 573.